ELSEVIER

Earth and Planetary Science Letters 210 (2003) 53–63

EPSL

www.elsevier.com/locate/epsl

Hypocenter depths of large interplate earthquakes and their relation to seismic coupling

Naoyuki Kato *, Tetsuzo Seno

Earthquake Research Institute, University of Tokyo, 1-1-1 Yayoi, Bunkyo-ku, Tokyo 113-0032, Japan

Received 15 October 2002; received in revised form 25 February 2003; accepted 28 February 2003

Abstract

We examine locations of hypocenters of large interplate earthquakes ($M \geq 7.5$) at subduction zones relative to their rupture areas to obtain a relation between the hypocentral depth and the seismic coupling coefficient, which is the ratio of the long-term slip rate estimated from cumulative seismic moment of large earthquakes to the relative plate motion. We find: (1) that the hypocentral depth is close to the bottom of the depth extent of the rupture area when the seismic coupling coefficient is nearly equal to 1.0; and (2) that the hypocentral depth relative to the depth extent of the rupture area shows a large scatter from shallow to deep when the seismic coupling coefficient is smaller than about 0.5. To interpret these observations, we conduct a numerical simulation of seismic cycles of interplate earthquakes where the frictional stress on the plate boundary is assumed to obey a laboratory-derived rate- and state-dependent friction law. The observed result (1) is reproduced in the simulation when the critical fault length, which is the size of the fault where the slip nucleation process takes place, is much shorter than the seismogenic zone of the plate boundary. In this case, the plate boundary is strongly locked during an interseismic period, and accordingly the calculated seismic coupling coefficient is close to 1.0. Seismic slip starts near the bottom of the seismogenic zone, because the maximum shear-stress concentration is generated near the bottom of the seismogenic zone due to deeper steady plate motion. On the other hand, when the critical fault length is large, appreciable aseismic sliding occurs in the seismogenic zone and, therefore, the calculated seismic coupling coefficient becomes significantly smaller than 1.0. The hypocentral depths of simulated large earthquakes tend to be shallow for large critical fault lengths. Heterogeneous frictional properties on the plate boundary may produce non-uniform aseismic sliding during an interseismic period. In this case, the seismic coupling is small and seismic slip starts in various portions of the seismogenic zone. This can explain the observed result (2).

Keywords: subduction zone; hypocenter depth; seismic coupling; friction; numerical simulation

1. Introduction

Kelleher et al. [1] reported that the epicenters of large interplate earthquakes at subduction zones are usually located near the landward sides of the aftershock zones, indicating that the seismic rupture often starts near the bottom of the rupture

* Corresponding author. Tel.: +81-3-5841-5812; Fax: +81-3-5689-7234.
E-mail addresses: nkato@eri.u-tokyo.ac.jp (N. Kato), seno@eri.u-tokyo.ac.jp (T. Seno).

0012-821X/03/$ – see front matter
doi:10.1016/S0012-821X(03)00141-9

area and propagates upward. Sibson [2] pointed out the same thing for large inland earthquakes in the United States. These observational facts may indicate that in many cases shear strength is largest at the bottom of the seismogenic zone, below which stable sliding or shear flow is thought to take place (e.g. Sibson [2], Das and Scholz [3]). On the other hand, many exceptions are known. For example, the hypocenters of the 1968 Tokachi-oki earthquake ($M_w = 8.3$) and the 1994 Sanriku-oki earthquake ($M_w = 7.7$), which occurred in the subduction zone along the Japan trench, were located near the trench axis and their rupture propagated downward (e.g. Sato et al. [4], Nagai et al. [5]). The epicenter of the 1978 Oaxaca, Mexico, earthquake ($M_w = 7.6$) is located near the center of the down-dip width of the aftershock zone [6]. It is known that the seismic coupling coefficient, which is defined by the ratio of the seismic slip rate estimated from the cumulative seismic moment of large interplate earthquakes to the relative plate velocity, is small for the Japan and Mexico subduction zones (e.g. Peterson and Seno [7]). This indicates that a significant amount of aseismic sliding takes place at the seismogenic depths on the plate boundary in these zones. If a significant amount of aseismic sliding occurs and its spatial distribution is non-uniform on the seismogenic plate boundary, shear-stress concentration does not necessarily occur at the bottom of the seismogenic zone, and then the hypocentral depths of large interplate earthquakes would be located at various positions of the seismogenic zone.

Rate- and state-dependent friction laws developed by Dieterich [8] and Ruina [9] on the basis of laboratory studies of rock friction may properly describe both seismic and aseismic slip observed in the laboratory (e.g. Marone [10]). The laws have successfully been applied to modeling of seismic cycles on plate boundaries since Tse and Rice [11] presented a model for the San Andreas fault, California. Because the rate- and state-dependent friction laws can simulate aseismic sliding in pre-, post-, and inter-seismic periods at a certain level of agreement with field data, they may be useful for understanding seismic coupling [12,13].

In the present paper, we examine the relation between the hypocentral depths of large interplate earthquakes at subduction zones and the seismic coupling coefficients. We also perform a numerical simulation of interplate earthquake cycles at a subduction zone using a rate- and state-dependent friction law to explore the physical mechanism of the above relation.

2. Observed relation

Using published data, we examine the locations of epicenters relative to rupture areas of large interplate earthquakes at subduction zones. Because we focus on the hypocentral depths of large interplate earthquakes relative to the seismogenic depths, we exclude from the present analysis earthquakes whose rupture area dimensions are small compared to the down-dip width of the seismogenic zone. Here, the seismogenic zone is defined by the region where seismic slip takes place on the plate boundary, and it is between the shallow aseismic zone of soft unconsolidated gouge materials and the deep aseismic zone of high temperatures (e.g. Tichelaar and Ruff [14]). We then use 26 interplate earthquakes with $M_w \geq 7.5$ (Table 1), because their rupture areas cover nearly the entire seismogenic zone. In the present analysis, the rupture areas for most earthquakes were estimated from their aftershock areas. For the 1944 Tonankai, the 1946 Nankai, and the 1996 and 2001 Peruvian earthquakes, we use the estimates of rupture area from waveform inversions of their rupture processes. The references to the main shock epicenters, their seismic moments and rupture areas we use are listed in Table 1. For each pair of the epicenter of a main shock and its rupture area, we measure the width W of the rupture area and the distance D from the trenchward edge of the rupture area to the epicenter (inset in Fig. 1). The relative hypocentral location $d = D/W$ may accurately represent the hypocentral depth as a fraction of the seismogenic depth range when the rupture area covers nearly the entire seismogenic zone of the plate boundary and the dip angle of the plate boundary is nearly constant. The values of d determined are shown in Table 1. It is

Table 1
Relative depths d of large interplate earthquakes ($M_w \geq 7.5$) at subduction zones and the seismic coupling coefficient α

Event	Subduction zone	Date	M_w	d	α(PS)	α(PSS)	Reference
Tonankai	Nankai	12/07/1944	7.9	1.0	1.00[a]	–	[30,31]
Nankai	Nankai	12/20/1946	8.2	0.1	1.00[a]	–	[32,33]
Kamchatka	Kamchatka	11/04/1952	9.0	1.0	0.67	0.39	[14]
Andreanof Is.	Aleutian, east	03/09/1957	9.1	0.9	0.84	0.35	[14]
Guerrero	Mexico	07/28/1957	7.7	1.0	0.38	0.24	[14,34]
Chile	Chile, south	05/22/1960	9.5	1.0	1.57	–	[35]
Kuril	Kuriles, south	10/13/1963	8.3	0.9	0.36	1.45	[14]
Alaska	Alaska	03/28/1964	9.2	1.0	0.77	–	[36]
Rat Island	Aleutian, west	03/09/1965	8.7	0.7	0.31	1.12	[14]
Vanuatu	Vanuatu	08/01/1965	7.5	0.0	0.16	0.15	[37]
Oaxaca	Mexico	08/23/1965	7.5	0.95	0.38	0.24	[6]
Peru	Peru, south	10/17/1966	8.2	0.5	0.16	–	[38]
Tokachi-oki	Japan	05/16/1968	8.3	0.0	0.24	0.22	[5]
Kuril	Kuriles, south	08/11/1969	8.2	0.95	0.36	1.45	[14]
Varparaiso	Chile, central	07/08/1971	7.7	1.0	0.14	0.16	[39]
Kuril	Kuriles, south	06/17/1973	7.8	1.0	0.36	1.45	[14]
Oaxaca	Mexico	11/29/1978	7.6	0.5	0.38	0.24	[6]
Colombia	Colombia	12/12/1979	8.2	0.8	0.33	–	[40]
Varparaiso	Chile, central	03/03/1985	8.0	0.8	0.14	0.16	[39]
Michoacan	Mexico	09/19/1985	8.0	0.8	0.38	0.24	[14]
Andreanof Is.	Aleutian, east	05/07/1986	7.9	1.0	0.84	–	[14]
Antofagasta	Chile, central	03/05/1987	7.5	0.8	0.14	0.16	[39]
Sanriku-oki	Japan	12/28/1994	7.7	0.0	0.24	0.22	[5]
Antofagasta	Chile, central	07/30/1995	8.0	0.7	0.14	0.16	[39]
Peru	Peru, south	11/12/1996	7.7	0.3	0.16	–	[41]
Peru	Peru, south	06/23/2001	8.2	0.55	0.16	–	[42]

α(PS) and α(PSS) are from Peterson and Seno [7] and Pacheco et al. [15], respectively.
References are for the moment magnitudes M_w, epicentral locations, and rupture areas of the large earthquakes.
[a] α value for the Nankai subduction zone is revised. See text.

difficult to precisely determine d values except for recent earthquakes recorded with dense seismic networks, mainly because rupture areas were poorly constrained due to small numbers of aftershocks and their location errors. Since great earthquakes occur infrequently at very strongly coupled plate boundaries, we cannot get enough data if we exclude earthquakes with poor aftershock locations from the present analysis. However, even if errors in d are around 0.2, the conclusion of the present study is unchanged.

Peterson and Seno [7] and Pacheco et al. [15] determined seismic coupling coefficients for subduction zones. The seismic coupling coefficient α is defined by:

$$\alpha = V_s / V_{pl} \quad (1)$$

where V_s is the seismic slip rate estimated from the seismic moment of large interplate earthquakes, divided by the width of the seismogenic zone and the recurrence time, and V_{pl} is the slip rate calculated from relative plate motions. Peterson and Seno [7] and Pacheco et al. [15] found that α varies significantly with locality as shown in Table 1, where α(PS) values are taken from table 2 of Peterson and Seno [7] and α(PSS) from table 4 of Pacheco et al. [15]. In Table 1, we follow Peterson and Seno [7] to assign subduction-zone names. Each α(PSS) value in Table 1 is the average value of α for blocks in the corresponding subduction zone of Peterson and Seno [7]. The α value for the Nankai subduction zone determined by Peterson and Seno [7] is 0.5, where they assumed the lower depth limit of coupling to be 60 km. Ozawa et al. [16], however, found from recent GPS observations that the plate boundary along the Nankai trough is strongly locked, suggesting that the seismic coupling coefficient in this

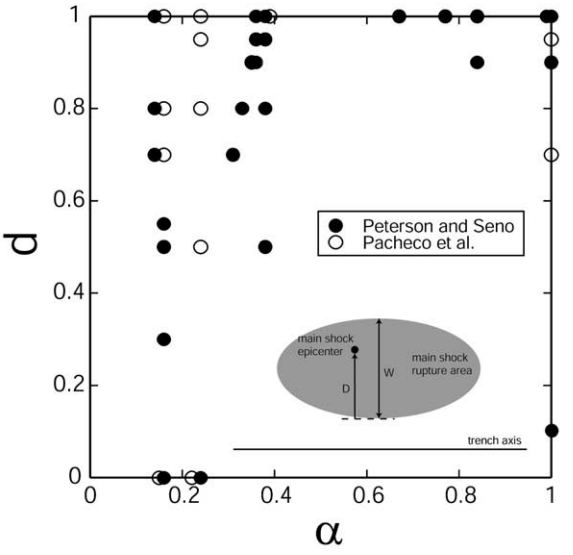

Fig. 1. The relative hypocentral depth d versus the seismic coupling coefficient α obtained for large interplate earthquakes at subduction zones (Table 1). Solid and open circles stand for α values from Peterson and Seno [7] and from Pacheco et al. [15], respectively. When α is estimated to be greater than 1 (Table 1), it is reduced to 1. The relative hypocentral depth d is defined by D/W, where D is the distance from the trenchward edge of the rupture area to the epicenter and W is the width of the rupture area in the direction perpendicular to the trench axis (inset).

region is close to 1.0. Recent studies indicated that the lower depth limit for coupling at the Nankai region is around 30 km (e.g. Hyndman et al. [17]). We then correct the α(PS) value to be 1.0 for the Nankai subduction zone.

Fig. 1 shows the obtained relation between the relative hypocentral depth d and the seismic coupling coefficient α. The estimated α values (Table 1) are sometimes larger than 1.0 because the estimated values of V_s may have large errors since the history of instrumental measurements of earthquakes is not long enough to cover several seismic cycles. Since $\alpha > 1$ is physically unreasonable, data with $\alpha > 1$ are plotted as $\alpha = 1$ in Fig. 1. When α is larger than about 0.5, d is close to 1.0 except for the 1946 Nankai earthquake, which will be discussed at the end of the next section. d shows a large scatter, viz. its full possible range, for $\alpha < \sim 0.5$, but is tightly grouped for $\alpha > 0.6$ (except for one or two points). This observed relation indicates that when the seismic coupling coefficient is high and therefore the plate boundary is strongly locked during an interseismic period, the seismic rupture of large interplate earthquakes starts near the bottom of the seismogenic zone. In contrast, when the seismic coupling coefficient is smaller and therefore a significant amount of aseismic sliding occurs at the seismogenic depths of the plate boundary, aseismic sliding at seismogenic depths affects the rupture initiation point of a large interplate earthquake and the depth of the initiation point of seismic rupture of a large interplate earthquake is not necessarily close to the bottom of the seismogenic zone.

3. Interpretation of the observed relation: numerical simulation

In order to physically understand the observed relation between the hypocenter depth of a large interplate earthquake and the seismic coupling coefficient, we perform a numerical simulation of seismic cycles at a subduction zone. The frictional stress on the plate boundary is taken to obey a rate- and state-dependent friction law [8,9], which has been successfully applied to modeling of seismic cycles (e.g. Tse and Rice [11], Stuart [18], Stuart and Tullis [19], Kato and Hirasawa [13]). The rate- and state-dependent friction law simulates aseismic sliding as well as coseismic slip and frictional healing, producing seismic cycles similar to actual ones. Aseismic sliding is particularly important to the discussion of the seismic coupling [13].

The simulation method is essentially the same as those in preceding studies (e.g. Kato and Hirasawa [13], Kato and Tullis [20]). We consider a two-dimensional model for a subduction zone in a uniform elastic half-space. A thrust fault with a dip angle of 20° is regarded as the boundary between a subducting oceanic plate and an overriding continental plate. The ξ axis is taken along the plate boundary and $\xi = 0$ is at the free surface. The frictional stress for $0 \leq \xi \leq 200$ km on the plate boundary is assumed to obey a rate- and state-dependent friction law. Stable sliding with slip rate equal to $V_{pl} = 10$ cm/yr is assumed for $\xi > 200$ km.

The plate boundary with $\xi \leq 200$ km is divided into a number of cells, each of which has uniform slip. The shear stress at the center of the ith cell on the plate boundary due to slip is written as:

$$\tau_i(t) = \sum K_{ij}[u_j(t) - V_{\mathrm{pl}}t] - (G/2c)(\mathrm{d}u_i/\mathrm{d}t) \quad (2)$$

where u_j is slip on the jth cell, K_{ij} relates slip on the jth cell to static shear stress on the ith cell and is given theoretically by Rani and Singh [21], G is rigidity, and c is the S-wave speed. The second term on the right-hand side of Eq. 2 represents radiation damping, which was introduced by Rice [22] to approximately evaluate the reduction of shear stress during seismic slip. By introducing this term, slip behavior for all parts of seismic cycles can be calculated.

Among several versions of rate- and state-dependent friction law, we apply the composite law proposed by Kato and Tullis [20,23]. The frictional stress is given by:

$$\tau = \mu \sigma_{\mathrm{n}}^{\mathrm{eff}} \quad (3)$$

$$\mu = \mu_* + a\ln(V/V_*) + b\ln(V_*\theta/L) \quad (4)$$

$$\mathrm{d}\theta/\mathrm{d}t = \exp(-V/V_{\mathrm{c}}) - (\theta V/L)\ln(\theta V/L) \quad (5)$$

where μ is the friction coefficient, $\sigma_{\mathrm{n}}^{\mathrm{eff}}$ is the effective normal stress, V is the sliding velocity, θ is a state variable, and a, b, L and V_{c} are constants. The characteristic slip distance L represents slip dependence and a and b represent rate dependence of frictional stress. V_{c} represents the cutoff velocity, below which time-dependent healing effectively occurs. Following Kato and Tullis [20,23], we take $V_{\mathrm{c}} = 10^{-8}$ m/s. If we use other kinds of rate- and state-dependent friction laws, simulated seismic cycles are qualitatively similar [20]. Performing some numerical simulations with the slip law and the slowness law, which are popular versions of rate- and state-dependent law [24], we confirm that the conclusion of the present study holds.

When $a-b<0$, the steady-state frictional stress decreases with an increase in slip velocity. This can lead to seismic slip, according to theoretical linear stability analyses (e.g. Ruina [9]). Under this condition, seismic slip tends to occur more easily for a smaller value of L because stress decreases more rapidly with slip. Only stable sliding occurs when $a-b>0$. The variations with depth of A, B, and $A-B$ assumed in the present study are shown in Fig. 2, where $A = a\sigma_{\mathrm{n}}^{\mathrm{eff}}$, $B = b\sigma_{\mathrm{n}}^{\mathrm{eff}}$, and $\sigma_{\mathrm{n}}^{\mathrm{eff}}$ is the effective normal stress given by the difference between the normal stress applied to the fault and the pore fluid pressure. $A-B$ is negative at depths from 6.0 to 43.6 km. This region may approximately correspond to the seismogenic zone, where earthquakes take place. A similar depth dependence of A and B has been applied for seismic cycle simulations (e.g. Stuart [18], Kato and Hirasawa [13]), because the friction parameters vary with depth due to temperature variation [25] and interplate earthquakes at subduction zones are confined approximately at these depths (e.g. Tichelaar and Ruff [14], Pacheco et al. [15]). The characteristic slip distance L is assumed to be uniform over the plate boundary. We vary L from 1 to 30 cm.

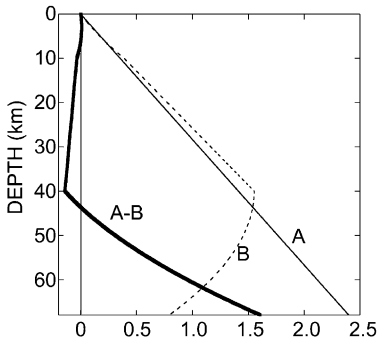

Fig. 2. The depth dependence of frictional constitutive parameters A (thin solid line), B (dotted line), and $A-B$ (thick solid line) assumed in the simulation.

When friction obeys a rate- and state-dependent friction law, a critical size h^* of slip nucleation exists [26,27]. Accelerating aseismic sliding in the slip nucleation zone precedes an earthquake, and the amplitude of preseismic sliding increases with h^*. For an in-plane shear crack in a 2-D uniform elastic medium, h^* is given by Dieterich [27] as follows:

$$h^* = 4GL/3(B-A) \quad (6)$$

In numerical simulations, the cell size h must be sufficiently smaller than h^*, as discussed by Rice [22], to prevent numerical instability. In the

present simulation, we use depth-dependent h values ranging from 50 m to 1 km because h^* varies with depth. The maximum value of $h/h^* = 0.018$ assures stability of the present simulation. Kato and Hirasawa [13] argued that the ratio of h^* to the $A-B<0$ zone width controls the seismic coupling coefficient. When h^* is larger than the $A-B<0$ zone width, seismic slip never occurs and therefore the seismic coupling coefficient ≈ 0. For a smaller h^*, a smaller amplitude of aseismic sliding precedes seismic slip, leading to a larger value of the seismic coupling coefficient. Scholz and Campos [12] found that the seismic coupling coefficient correlates with the estimated normal stress at the plate interface. Because h^* is inversely proportional to the normal stress, the finding by Scholz and Campos [12] can be elucidated by the above discussion of h^*.

The characteristics of simulated seismic cycles are essentially the same as those in preceding studies (e.g. Kato and Hirasawa [13]). Large earthquakes repeatedly occur at a constant recurrence interval T_r mainly in the $A-B<0$ region and significant postseismic and steady aseismic sliding occurs in the deeper $A-B>0$ region. As

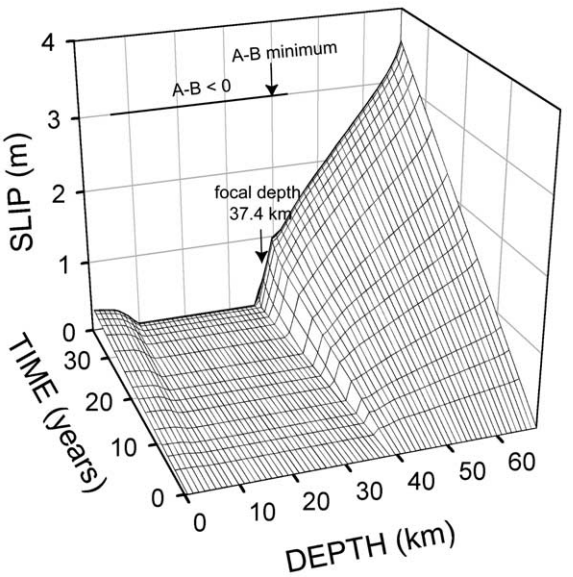

Fig. 3. Simulated slip distribution on a plate boundary for about 40 years prior to the occurrence of a large simulated earthquake in the case of $L = 2$ cm.

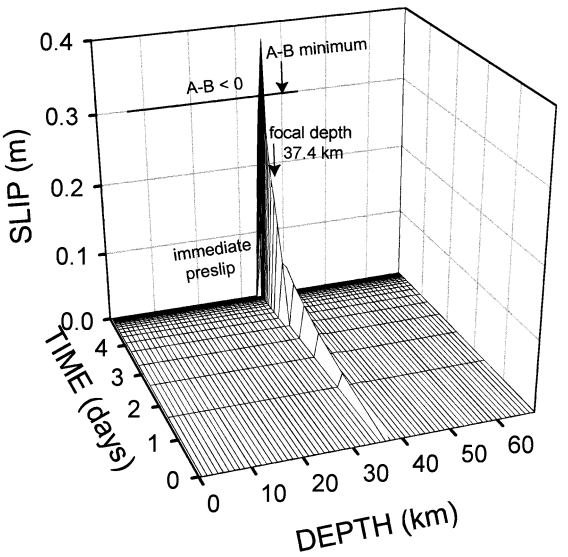

Fig. 4. Simulated slip distribution on a plate boundary for about 5 days immediately before a simulated earthquake in the case of $L = 2$ cm.

L increases, T_r increases and the seismic coupling coefficient decreases.

We examine the effects of L on simulated slip histories and characteristics of large earthquakes, using the simulation results for $L = 2$ cm and $L = 20$ cm. Fig. 3 shows simulated spatio-temporal variation of slip on the plate boundary for about 40 yr prior to a large earthquake in the case of $L = 2$ cm. Aseismic sliding occurs mainly in the deeper $A-B>0$ region, while the $A-B<0$ zone is virtually locked during an interseismic period. Aseismic sliding gradually penetrates into the $A-B<0$ zone, where large earthquakes are expected to occur. Large stress concentration is generated near the boundary between the deep stable sliding region and the locked region. We show in Fig. 4 simulated preseismic slip immediately before the earthquake occurs. We find that the immediate preslip is generated where stress concentration is generated by long-term aseismic sliding, as seen in Fig. 3. Dynamic rupture starts at a depth of 37.4 km near the deeper edge of the immediate preslip region, where we assume that the dynamic rupture starts when the slip velocity reaches 1 cm/s. This velocity criterion is arbitrarily chosen; however, the results change little if we

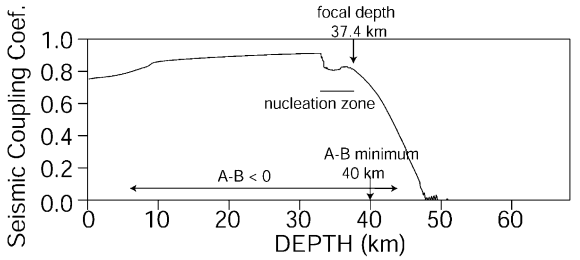

Fig. 5. Depth dependence of the seismic coupling coefficient α for a simulated seismic cycle in the case of $L=2$ cm.

take 1 mm/s or 10 cm/s as the velocity criterion for dynamic rupture. This result, that the slip nucleation occurs near the bottom of the $A-B<0$ zone, is consistent with the recent simulation result by Lapusta et al. [28], where L is assumed to be smaller than 1 cm.

The critical size h^* of slip nucleation defined by Eq. 6 is calculated to be 6.5 km when we use the $A-B$ value at a depth of 34.8 km, which is the middle depth of the slip nucleation zone (Fig. 5). The width of the preseismic slip zone measured in Fig. 4 is 15.2 km, which is about 2.3 times as large as the theoretical value. A similar discrepancy between the simulated and theoretical value is seen in the simulation results by Dieterich [27].

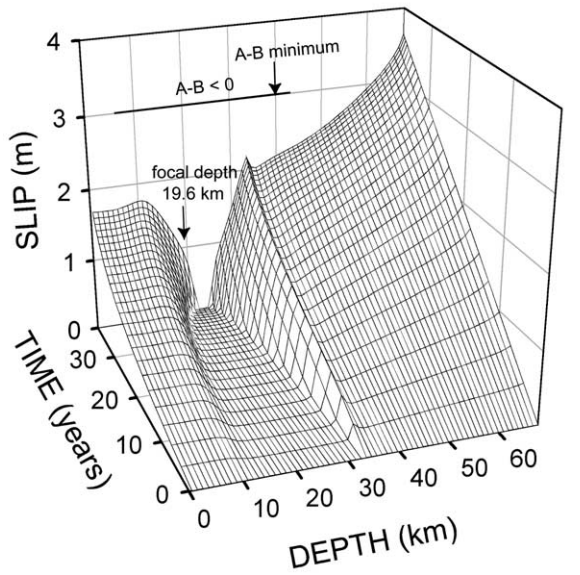

Fig. 6. Simulated slip distribution on a plate boundary for about 40 years prior to the occurrence of a large simulated earthquake in the case of $L=20$ cm.

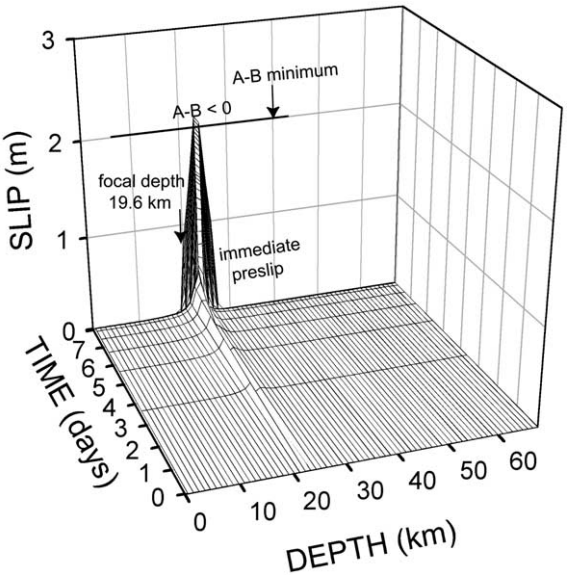

Fig. 7. Simulated slip distribution on a plate boundary for about 8 days immediately before a simulated earthquake in the case of $L=20$ cm.

The local seismic coupling coefficient defined by Eq. 1 is calculated at each depth for simulated seismic cycles, as shown in Fig. 5. Here, the seismic coupling coefficient α is given by $u_s/(V_{pl}T_r)$, where u_s is the seismic slip with a slip rate greater than or equal to 1 cm/s. The seismic coupling coefficient increases from 0 at depths greater than about 47 km, where $A-B$ is positive and significant aseismic sliding occurs during interseismic periods, to about 0.9 in the $A-B<0$ zone.

The simulation results in the case of $L=20$ cm are shown in Figs. 6–8. In this case, significant aseismic sliding occurs both in the shallower and deeper $A-B>0$ regions, and it propagates into the $A-B<0$ region. Rapid preseismic slip immediately before the earthquake occurs is generated when the stress concentration in the strongly locked region becomes large enough. Similar simulation results were observed in preceding studies (e.g. Tse and Rice [11], Stuart [18]). Fig. 7 shows simulated preseismic slip immediately before the earthquake occurs. In this case the dynamic rupture starts at a depth of 19.6 km near the shallower edge of the immediate preslip region rather

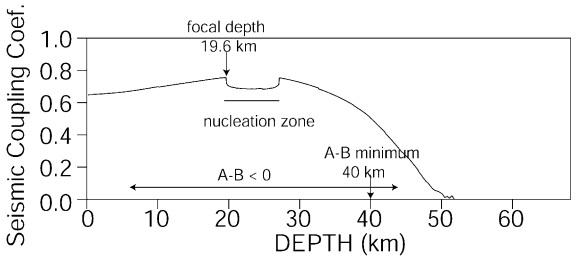

Fig. 8. Depth dependence of the seismic coupling coefficient α for a simulated seismic cycle in the case of $L=20$ cm.

than at the deeper edge. When L is large, the preslip region is large and also is located at shallow depths. Rupture tends to start at the shallower edge, probably because the interaction with the free surface makes the stress intensity factor there larger than that at the deeper edge [29]. The seismic coupling coefficient in this case (Fig. 8) is smaller than in the case of $L=2$ cm (Fig. 5), since significant aseismic sliding occurs even in the seismogenic zone during an interseismic period.

The relation between the seismic coupling coefficient α and the normalized hypocentral depth d for a number of different simulated earthquakes is shown in Fig. 9. Here the seismic coupling coefficient is the average value over the $A-B<0$ zone and the hypocentral depth is the location relative to the $A-B<0$ zone. When the seismic coupling coefficient is close to 1.0 in the simulation, the hypocentral depth of a simulated large interplate earthquake is close to the bottom of the $A-B<0$ zone, as explained for the simulation results in the case of $L=2$ cm. This explains the observations well. Although we show simulation results only of the effects of L with the depth profile of A and B shown in Fig. 2, we performed simulations with various depth profiles of A and B. The results indicate that for a smaller value of h^* the seismic coupling coefficient is closer to 1.0 and the hypocentral depth is closer to the bottom of the seismogenic zone.

As L increases, the hypocentral depth becomes shallower and the seismic coupling coefficient decreases, resulting in the negative correlation between the hypocentral depth and the seismic coupling coefficient. The simulation relation (Fig. 9) is similar to the observed one (Fig. 1) in the negative correlation. Although the hypocentral depth of a simulated large earthquake simply decreases with a decrease in the seismic coupling coefficient, the observed relation does not show such a clear tendency. This is probably because a small value of the seismic coupling coefficient at a subduction zone is not always caused by a large value of the critical size h^* of slip nucleation, as shown in the present simulation. For example, when the frictional property on the plate boundary is heterogeneous and there exist strongly coupled asperities surrounded by weakly coupled regions as illustrated in Fig. 10a, the average seismic coupling coefficient over the plate interface should be appreciably smaller than 1.0. During an interseismic period in this case, asperities are locked while aseismic sliding may occur in the surrounding regions, causing high stress concentration in the perimeters of the asperities (heavily shaded zones in Fig. 10a). In this situation, the dynamic rupture is expected to start near an edge of an asperity, which could be either the shallower or deeper edge, depending on the spatial distribution of asperities and the value of L. A great earthquake occurs when all the asperities are broken at once, while rupture of only one asperity results in a smaller earthquake. This suggests that on a plate boundary with a smaller seismic coupling coefficient many smaller interplate earthquakes may

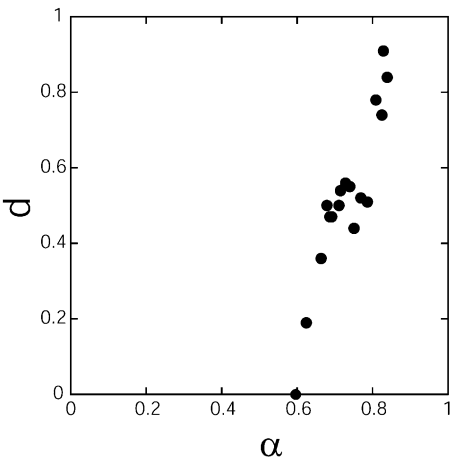

Fig. 9. The relative hypocentral depth d versus the seismic coupling coefficient α obtained from numerical simulations.

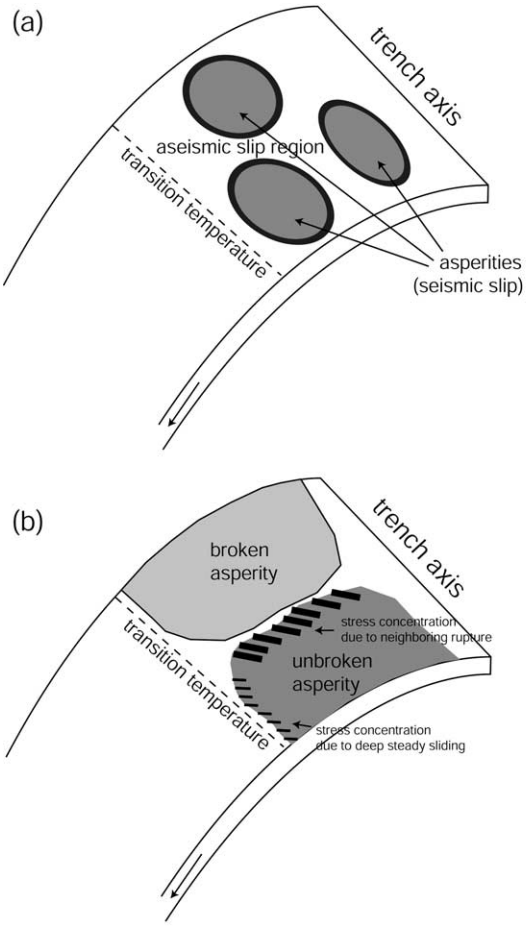

Fig. 10. (a) Illustration for heterogeneous plate boundary. Asperities (light gray regions) are strongly locked during an interseismic period, while aseismic sliding takes place in the surrounding regions. This causes stress concentration around the perimeters of the asperities (dark gray regions). (b) Illustration for successive rupture of neighboring asperities on a plate boundary with a high seismic coupling coefficient. Stress concentration by a previously broken asperity significantly affects the rupture initiation point of the unbroken asperity.

occur in addition to an occasional great earthquake.

It should be remarked that a shallow hypocentral depth of large interplate earthquake may occur exceptionally even when the seismic coupling coefficient is large. The hypocentral depth of the 1946 Nankai earthquake is located near the shallower edge of its rupture area ($d=0.1$; see Table 1), although the seismic coupling coefficient is large ($\alpha=1.0$). The 1946 Nankai earthquake occurred only 2 years after the 1944 Tonankai earthquake ($d=1$) took place at the eastern neighboring region in the same subduction zone. The hypocenter of the 1946 Nankai earthquake is located near the eastern edge of its rupture area. These facts indicate that the 1946 Nankai earthquake occurred under strong influence of the stress perturbation by the 1944 Tonankai earthquake. In this case, the stress concentration due to the neighboring earthquake may be dominant over the stress concentration due to deep aseismic sliding, as illustrated in Fig. 10b. Because the dynamic rupture of the unbroken asperity is expected to start from a place in the region of large stress concentration, the hypocenter is not necessarily near the bottom of the seismogenic zone.

4. Conclusion

We obtain a relation from published data between the seismic coupling coefficients and the hypocentral depths of large interplate earthquakes at subduction zones. This observed relation shows: (1) that the hypocentral depth is located near the bottom of the seismogenic zone when the seismic coupling coefficient is close to 1.0; and (2) that the hypocentral depth shows significant scatter when the seismic coupling coefficient is smaller than about 0.5.

The observed result (1) can be reproduced in a numerical simulation of seismic cycles with a rate- and state-dependent friction law. The simulation indicates that the $A-B<0$ zone of a plate boundary is strongly locked during interseismic periods, and the seismic coupling coefficient is large when the critical size h^* of slip nucleation is much smaller than the width of the $A-B<0$ zone. In this case, large stress concentration occurs near the bottom of the $A-B<0$ zone because aseismic sliding takes place below $A-B<0$ depths and therefore the ruptures of large interplate earthquakes start near the bottom of the $A-B<0$ zone.

Numerical simulation results further indicate that the hypocentral depths of large interplate earthquakes tend to be shallow when a significant

amount of aseismic sliding occurs in the $A-B<0$ zone during interseismic periods and therefore the seismic coupling coefficient is small because of a large value of h^*. Non-uniformity in frictional properties on the plate boundary may be responsible for the observed scatter of the hypocentral depths for the small seismic coupling coefficients. These may explain the observed result (2). In summary, the hypocentral depths of large interplate earthquakes are controlled by the frictional properties of the plate boundary, and therefore are correlated with the seismic coupling coefficient.

Acknowledgements

We are grateful to Lynn Sykes and William Stuart for careful reviews, which were useful in improving the manuscript. Numerical computation was partly done at the Earthquake Information Center, Earthquake Research Institute, University of Tokyo.*[SK]*

References

[1] J. Kelleher, L. Sykes, J. Oliver, Possible criteria for predicting earthquake locations and their application to major plate boundaries of the Pacific and the Caribbean, J. Geophys. Res. 78 (1973) 2547–2585.
[2] R.H. Sibson, Fault zone models, heat flow, and the depth distribution of earthquakes in the continental crust of the United States, Bull. Seismol. Soc. Am. 72 (1982) 151–163.
[3] S. Das, C.H. Scholz, Why large earthquakes do not nucleate at shallow depths, Nature 305 (1983) 621–623.
[4] T. Sato, K. Imanishi, M. Kosuga, Three-stage rupture process of the 28 December 1994 Sanriku-oki earthquake, Geophys. Res. Lett. 23 (1996) 33–36.
[5] R. Nagai, M. Kikuchi, Y. Yamanaka, Comparative study on the source processes of recurrent large earthquakes in Sanriku-oki Region: the 1968 Tokachi-oki earthquake and the 1994 Sanriku-oki earthquake, Zisin Ser. 2 54 (2001) 267–280.
[6] F. Tajima, K.C. McNally, Seismic rupture patterns in Oaxaca, Mexico, J. Geophys. Res. 88 (1983) 4263–4275.
[7] E.T. Peterson, T. Seno, Factors affecting seismic moment release rates in subduction zones, J. Geophys. Res. 89 (1984) 10233–10248.
[8] J.H. Dieterich, Modeling of rock friction 1. Experimental results and constitutive equations, J. Geophys. Res. 84 (1979) 2161–2168.
[9] A.L. Ruina, Slip instability and state variable friction laws, J. Geophys. Res. 88 (1983) 10359–10370.
[10] C. Marone, Laboratory-derived friction laws and their application to seismic faulting, Annu. Rev. Earth Planet. Sci. 26 (1998) 643–696.
[11] S.T. Tse, J.R. Rice, Crustal earthquake instability in relation to the depth variation of frictional slip properties, J. Geophys. Res. 91 (1986) 9452–9472.
[12] C.H. Scholz, J. Campos, On the mechanism of seismic decoupling and back arc spreading at subduction zones, J. Geophys. Res. 100 (1995) 22103–22115.
[13] N. Kato, T. Hirasawa, A numerical study on seismic coupling along subduction zones using a laboratory-derived friction law, Phys. Earth Planet. Inter. 102 (1997) 51–68.
[14] B.W. Tichelaar, L.J. Ruff, Depth of seismic coupling along subduction zones, J. Geophys. Res. 98 (1993) 2017–2038.
[15] J.F. Pacheco, L.R. Sykes, C.H. Scholz, Nature of seismic coupling along simple plate boundaries of the subduction type, J. Geophys. Res. 98 (1993) 14133–14159.
[16] T. Ozawa, T. Tabei, S. Miyazaki, Interplate coupling along the Nankai trough off southwest Japan derived from GPS measurements, Geophys. Res. Lett. 26 (1999) 927–930.
[17] R.D. Hyndman, K. Wang, M. Yamano, Thermal constraints on the seismogenic portion of the southwestern Japan subduction zone, J. Geophys. Res. 100 (1995) 15373–15392.
[18] W.D. Stuart, Forecast model for great earthquakes at the Nankai trough subduction zone, Pure Appl. Geophys. 126 (1988) 619–641.
[19] W.D. Stuart, T.E. Tullis, Fault model for preseismic deformation at Parkfield, California, J. Geophys. Res. 100 (1995) 24079–24099.
[20] N. Kato, T.E. Tullis, Numerical simulation of seismic cycles with a composite rate- and state-dependent friction law, Bull. Seismol. Soc. Am. (2003) in press.
[21] S. Rani, S.J. Singh, Static deformation of a uniform halfspace to a long dip-slip fault, Geophys. J. Int. 109 (1992) 469–476.
[22] J.R. Rice, Spatio-temporal complexity of slip on a fault, J. Geophys. Res. 98 (1993) 9885–9907.
[23] N. Kato, T.E. Tullis, A composite rate- and state-dependent law for rock friction, Geophys. Res. Lett. 28 (2001) 1103–1106.
[24] N.M. Beeler, T.E. Tullis, J.D. Weeks, The roles of time and displacement in the evolution effect in rock friction, Geophys. Res. Lett. 21 (1994) 1987–1990.
[25] M.L. Blanpied, D.A. Lockner, J.D. Byerlee, Frictional slip of granite at hydrothermal conditions, J. Geophys. Res. 100 (1995) 13045–13064.
[26] J.H. Dieterich, A model for the nucleation of earthquake slip, in: S. Das, J. Boatwright, C.H. Scholz (Eds.), Earthquake Source Mechanics, American Geophysical Union, Washington, DC, 1986, pp. 37–47.
[27] J.H. Dieterich, Earthquake nucleation on faults with rate-

and state-dependent strength, Tectonophysics 211 (1992) 115–134.
[28] N. Lapusta, J.R. Rice, Y. Ben-Zion, G. Zheng, Elastodynamic analysis for slow tectonic loading with spontaneous rupture episodes on faults with rate- and state-dependent friction, J. Geophys. Res. 105 (2000) 23765–23789.
[29] J.W. Rudnicki, M. Wu, Mechanics of dip-slip faulting in an elastic half-space, J. Geophys. Res. 100 (1995) 22173–22186.
[30] H. Kanamori, Tectonic implications of the 1944 Tonankai and the 1946 Nankaido earthquakes, Phys. Earth Planet. Inter. 5 (1972) 129–139.
[31] M. Kikuchi, M. Nakamura, K. Yoshikawa, Source rupture processes of the 1944 Tonankai earthquake and the 1945 Mikawa earthquake derived from low-gain seismograms, Earth Planet. Space (2003) in press.
[32] T. Hashimoto, M. Kikuchi, Source process of the 1946 Nankai earthquake as revealed from seismic records, Earth Mon. Spec. Ser. 24 (1999) 16–20.
[33] Y. Yamanaka, M. Kikuchi, K. Yoshikawa, Source processes of the 1946 Nankai earthquake (M8.0) and the 1964 Niigata earthquake (M7.5) inferred from JMA strong motion records, Abstr. Seismol. Soc. Jpn. (2001) C68.
[34] J.G. Anderson, S.K. Singh, J.M. Espindola, J. Yamamoto, Seismic strain release in the Mexican subduction thrust, Phys. Earth Planet. Inter. 58 (1989) 307–322.
[35] G. Plafker, J.C. Savage, Mechanism of the Chilean earthquakes of May 21 and 22 1960, Geol. Soc. Am. Bull. 81 (1970) 1001–1030.
[36] H. Kanamori, The Alaska earthquake of 1964: Radiation of long-period surface waves and source mechanism, J. Geophys. Res. 75 (1970) 5029–5040.
[37] J.E. Ebel, Source processes of the 1965 New Hebrides islands earthquakes inferred from teleseismic waveforms, Geophys. J. R. Astron. Soc. 63 (1980) 381–403.
[38] K. Abe, Mechanisms and tectonic implications of the 1966 and 1970 Peru earthquakes, Phys. Earth Planet. Inter. 5 (1972) 367–379.
[39] D.A. Oleskevich, R.D. Hyndman, K. Wang, The updip and downdip limits to great subduction earthquakes: thermal and structural models of Cascadia, south Alaska, SW Japan, and Chile, J. Geophys. Res. 104 (1999) 14965–14991.
[40] S.L. Beck, L.J. Ruff, The rupture process of the great l979 Colombia earthquake: evidence for the asperity model, J. Geophys. Res. 89 (1984) 9281–9291.
[41] M. Kikuchi, Y. Yamanaka, The Peru earthquake on November 12, 1996 (Ms 7.3), EIC Earthquake Note No. 7 (1996).
[42] M. Kikuchi, Y. Yamanaka, The Peru earthquake on June 23, 2001 (Mw 8.2), EIC Earthquake Note No. 105 (2001).